



OPEN

Nonlinear dispersion relation in integrable turbulence

Alexey Tikan^{1,6}, Félicien Bonnefoy², Guillaume Ducroz², Gaurav Prabhudesai³, Guillaume Michel⁴, Annette Cazaubiel⁵, Éric Falcon⁵, Francois Copie¹, Stéphane Randoux¹ & Pierre Suret¹✉

We investigate numerically and experimentally the concept of nonlinear dispersion relation (NDR) in the context of partially coherent waves propagating in a one-dimensional water tank. The nonlinear random waves have a narrow-bandwidth Fourier spectrum and are described at leading order by the one-dimensional nonlinear Schrödinger equation. The problem is considered in the framework of integrable turbulence in which solitons play a key role. By using a limited number of wave gauges, we accurately measure the NDR of the slowly varying envelope of the deep-water waves. This enables the precise characterization of the frequency shift and the broadening of the NDR while also revealing the presence of solitons. Moreover, our analysis shows that the shape and the broadening of the NDR provides signatures of the deviation from integrable turbulence that is induced by high order effects in experiments. We also compare our experimental observations with numerical simulations of Dysthe and of Euler equations.

Nonlinear dispersion relation (NDR) (i.e. the relation between wavevectors k and angular frequencies ω for waves of finite amplitude) is a powerful tool to highlight dynamical and spectral properties of nonlinear wave fields^{1–3}. The concept of NDR is relevant to all the fields of Physics where the Fourier modes provide a relevant basis to describe the waves and their interactions (nonlinear optics⁴, hydrodynamics^{2,3,5}, hydroelasticity⁶, mechanics¹, quantum optics⁷, plasma physics^{8,9},...). In particular, it has been extensively used in the context of wave turbulence (WT), where the interaction between random nonlinear waves is dominated by resonances among random Fourier components^{1–3,10–12}.

On the other hand, systems of nonlinear random waves governed by integrable partial differential equations such as the Korteweg de Vries, sine-Gordon or the one-dimensional nonlinear Schrödinger equation (1DNLSE) represent a profoundly different class of problems because the natural basis for the analysis is provided by the inverse scattering transform (IST) sometimes called “nonlinear Fourier transform”¹³. In this framework, the field is decomposed into two components—the radiation and the solitons—identified with two types of nonlinear spectra—the continuous spectrum and the discrete spectrum respectively¹⁴.

Integrable wave systems exhibit a remarkable form of turbulence called “integrable turbulence” (IT)^{15–19}. In particular, while exact and non trivial resonances play a crucial role in WT, they are not allowed in IT (see²⁰ and “Methods”). Moreover, in WT, spectra are often characterized by power laws while the known spectra in IT exhibit exponential tails²¹. Soliton gas recently investigated in water waves experiments represents a peculiar “purely solitonic” case of IT^{22–24}. However, IT more generally involves the interplay between nonlinear radiation (dispersive waves) and solitons. While these two components are naturally distinguished within the framework of IST, they cannot be easily separated in the physical space. Even if IT and WT regimes are of strongly different natures, the possibility to analyse IT and to reveal the existence of solitons by using conventional tools such as the NDR (instead of the complicated machinery of IST) is of crucial importance from the practical and fundamental point of views²³.

Surprisingly, despite the universality of the 1DNLSE, little attention has been paid to its NDR up to a very recent theoretical study²⁵ in which various kinds of initial conditions have been investigated. In this interesting work, the authors show that the NDR of weakly nonlinear random waves only experiences the well-known frequency shift^{26,27}, while the NDR of a single soliton is a straight line having a slope corresponding to its group velocity (see “Methods”)^{25,28}. To the best of our knowledge, the concept of NDR has not been applied to IT

¹Univ. Lille, CNRS, UMR 8523, PhLAM - Physique des Lasers Atomes et Molécules, F-59000 Lille, France. ²École Centrale de Nantes, LHEEA, UMR 6598, CNRS, 44 321 Nantes, France. ³LPENS, Ecole Normale Supérieure, CNRS, PSL Research University, Sorbonne Université, Université Paris Cité, F-75005 Paris, France. ⁴Institut Jean Le Rond d’Alembert, UMR 7190, CNRS, Sorbonne Université, 75 005 Paris, France. ⁵Université Paris Cité, CNRS, MSC, UMR 7057, F-75013 Paris, France. ⁶Present address: Institute of Physics, Swiss Federal Institute of Technology Lausanne (EPFL), 1015 Lausanne, Switzerland. ✉email: Pierre.Suret@univ-lille.fr

experiments described at leading order by 1DNLSE. In particular the (Fourier) spectral signature of solitons has not been reported in this context.

In this manuscript, we first use numerical simulations of 1DNLSE to investigate the NDR and the power spectral density -PSD- (in the space-time (ω, k) Fourier plane) in IT. We show that the PSD and the NDR present clear signature of the growing influence of solitons when the nonlinearity strength is increased. We then report on an experiment in which partially coherent (random) deep water surface gravity waves propagate along a long one-dimensional flume. We demonstrate that removing the carrier wave enables the accurate measurement of the NDR of wavefields having a narrow Fourier spectrum by using a very limited number of gauges. In experiments, the NDR is found to reveal both the existence of solitons embedded in the random field and a deviation from IT induced by higher-order nonlinear effects not taken into account in the 1DNLSE model. Simulations of Euler and Dysthe equations confirm the influence of high order terms and provide a deeper insight into the mechanisms behind the formation of coherent structures observed in the experiment.

Results

Numerical simulations (nonlinear Schrödinger equation). Considering unidirectional deep water gravity waves having a narrow spectrum, the surface elevation $\eta(\tau, z)$ is:

$$\eta(\tau, z) = \frac{1}{2} \left(\psi_r(\tau, z) e^{i(k_0 z - \omega_0 \tau)} + c.c. \right); \quad (1)$$

where ψ_r is the slowly-varying complex envelope, $f_0 = \omega_0 / (2\pi)$ and $k_0 = \omega_0^2 / g$ are the frequency and the modulus of the wavevector of the carrier wave respectively, z is the propagation distance and τ is the time measured in the laboratory frame. For deep water gravity waves, the dynamics of $\psi(t, z) = \psi_r(\tau, z)$ is described at leading order by the focusing 1DNLSE²⁹:

$$i \frac{\partial \psi}{\partial z} = \frac{1}{g} \frac{\partial^2 \psi}{\partial t^2} + \gamma |\psi|^2 \psi, \quad (2)$$

where $t = \tau - z/c_g$, $c_g = g / (2\omega_0)$ is the group velocity evaluated at the frequency f_0 , $\gamma = k_0^3$ and g is the gravity acceleration. In simulations and in experiments, the initial conditions are partially coherent waves produced from the linear superposition of numerous independent Fourier components having a Gaussian spectrum (see “Methods” and^{19,21,30}). It is useful to introduce the degree of nonlinearity of the wave propagation, which is given by the parameter Γ :

$$\Gamma = \frac{\gamma g P_0}{(2\pi \Delta f)^2} \quad \text{with } P_0 = \langle |\psi(t, z = 0)|^2 \rangle \quad (3)$$

where $\Delta f \ll f_0$ is the initial spectral bandwidth evaluated at $z = 0$ and where $\langle \dots \rangle$ denotes the averaging over time and/or realizations. Note that $\langle |\psi|^2 \rangle = 2 \langle \eta^2 \rangle$ and that $\Gamma = BFI^2$ where BFI is the Benjamin-Feir Index^{31,32} (see “Methods”). It has been shown that large values of Γ lead to the formation of rogue waves characterized by heavy-tailed statistical distributions of the surface elevation^{16,19,30,31,33–35}.

We have first performed numerical simulations of Eq. (2) for three values of Γ (see “Methods” for details). Fig. 1a, represents the typical spatio-temporal dynamics of IT developing from partially coherent waves in the focusing regime of 1DNLSE. Remarkably, the number of isolated pulses emerging in the random wave field increases with the nonlinearity. Note that our numerical simulations reveal the presence of elastic collisions (see for the example the white circle in Fig. 1), a signature of solitons in integrable systems¹³.

We define the space-time double Fourier transform as:

$$\tilde{\psi}(\omega, k) = \iint \psi(t, z) e^{+i\omega t} e^{-ikz} dt dz \quad (4)$$

The power spectrum (PSD) $|\tilde{\psi}(\omega, k)|^2$ of one realization of $\psi(z, t)$ is plotted in blue in Fig. 1b. As pointed out in²⁵ and reported below in “Methods”, the straight lines in the $k - \omega$ space are signature of the solitons observed in the spatio-temporal dynamics (Fig. 1a). Note that the theoretical description of the statistical distribution of the slopes of the straight lines—associated to the velocities of the solitons—is a theoretical open question. We also plot the spectrum $\langle |\tilde{\psi}(\omega, k)|^2 \rangle$ averaged over several realizations in Fig. 1c. The linear dispersion of 1DNLSE reads $k(\omega) = \omega^2 / g$ ³⁶ and is plotted in dashed black lines in Fig. 1b,c. The NDR can be defined as the peak wavevectors \tilde{k} of the PSD for each value of ω in the (ω, k) plane²⁵. For moderate nonlinearities and narrow Fourier spectra, the nonlinear NDR gets shifted from the linear one and reads^{25,36}:

$$\tilde{k}(\omega, P_0) = k(\omega) - 2\gamma P_0. \quad (5)$$

As expected from Eq. (5), the NDR computed from numerical simulations shifts toward negative values of k (see red dashed lines in Fig. 1b,c). The Fig. 1c,d show that, the PSD broadens around the NDR when Γ increases because of the energy exchange among Fourier modes. This broadening phenomenon is well-known in standard WT with resonant interactions^{1–3,37} but, to the best of our knowledge, it has not been reported in IT where resonances are forbidden (see “Methods”).

The k -spectrum at $\omega = 0$, i.e. $n_k = \langle |\tilde{\psi}(0, k)|^2 \rangle$ is plotted in Fig. 1d. For small values of Γ , the maximum of this curve coincides with the value predicted by the weakly nonlinear theory (i.e. Eq. (5), red dashed line in Fig. 1d). Note that, in this weakly nonlinear regime, n_k can be empirically fitted by a Lorentzian distribution (purple dashed line in Fig. 1d). To the best of our knowledge, this remarkable fact, not known yet in IT, has

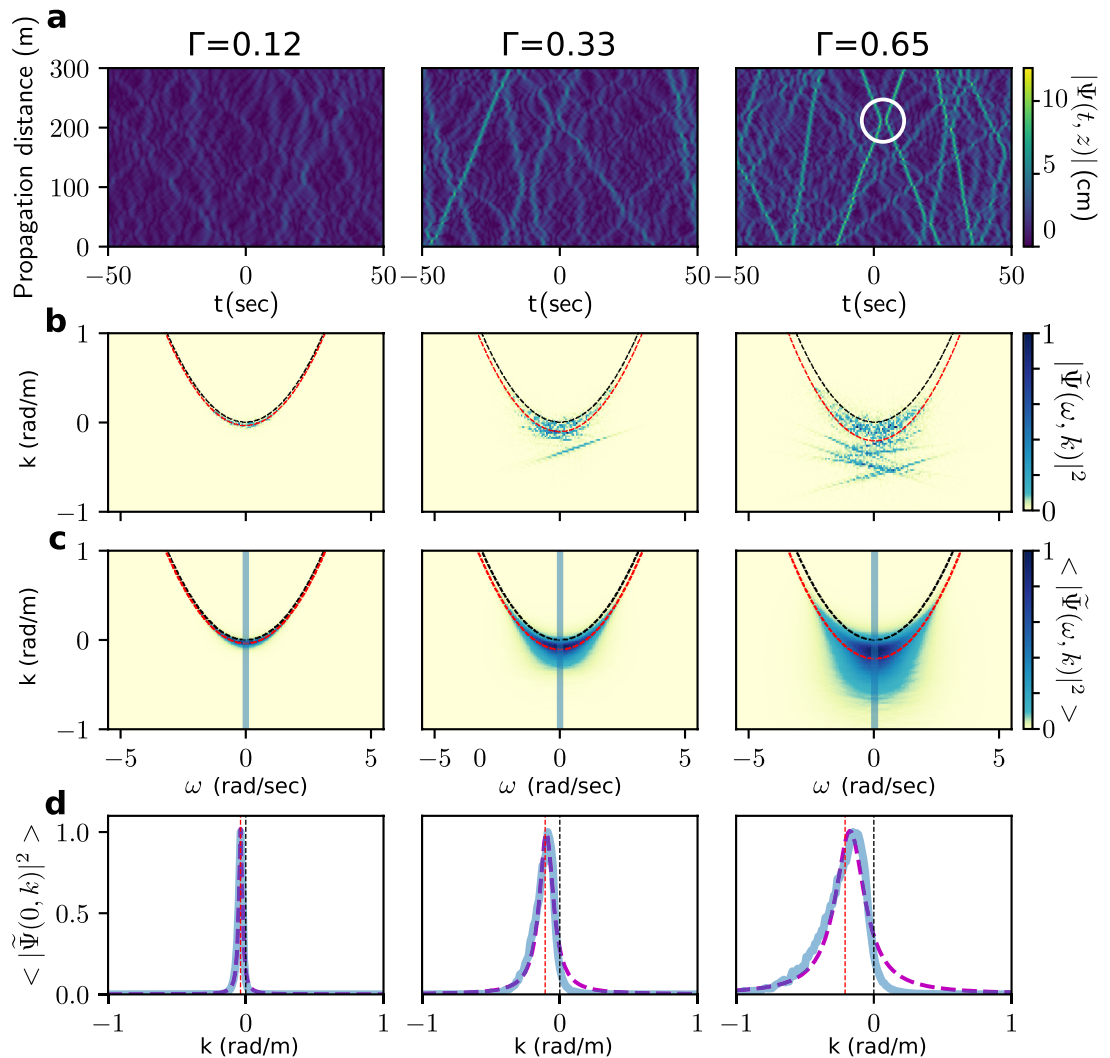


Figure 1. Numerical simulations of the 1-D NLS equation. Three columns correspond to three different values of Γ 0.12, 0.33, and 0.65, respectively. The central frequency of the carrier wave and the initial width of the wave spectrum are set to $f_0 = 1.15$ Hz and $\Delta f = 0.2$ Hz. **(a)** Spatiotemporal diagram for the complex envelope amplitude $|\psi(t, z)|$. **(b)** Corresponding nonlinear dispersion relation $|\tilde{\psi}(\omega, k)|^2$ normalized to the maximum. **(c)** Nonlinear dispersion relation averaged over 1000 realizations and normalized to the maximum. Propagation distance is 500 m. **(d)** Cross-section of the averaged nonlinear dispersion relation at $\omega = 0$ (along the blue line in c). Dashed purple line shows a Lorentzian fit. In **(b–d)**, vertical black and red dashed lines represent the linear dispersion $k(\omega)$ and its nonlinear correction of Eq. (5) respectively.

not been described theoretically. At higher nonlinearities, the number of straight lines associated with solitons (individually observed in Fig. 1a,b for $\Gamma = 0.65$) increases. The NDR of a single soliton follows the straight line $k = c_s \omega + (k_s - c_s \omega_s - \frac{1}{2} \gamma |\psi_0|^2)$ where c_s is the group velocity of the soliton in the (t, z) plane, ω_s is the central frequency of the soliton and $k_s = k(\omega_s) = \omega_s^2/g$ follows the linear dispersion (see²⁵ and “Methods”). As a consequence, the nonlinear phase shift acquired by solitons during their propagation places the solitonic lines well below the dispersion parabola described by Eq. (5) (see Fig. 1b).

Consequently, the strong and asymmetric broadening of the PSD profile n_k toward negative values of k (Fig. 1d) can be considered as a signature of the increasing number of solitons in the strongly nonlinear regime of IT.

Experiments. In order to investigate experimentally the NDR described above, we have used the setup described in³⁸ and schematically shown in Fig. 2a. Regimes close to IT can be achieved in unidirectional deep water waves having a narrow Fourier spectrum. Such waves are generated at one end of a 148 m long, 5 m wide and 3 m deep wave flume by a computer-assisted flap-type wavemaker (see Fig. 2a). The flume is equipped with an absorbing device strongly reducing wave reflection at the opposite end³⁸. The surface elevation $\eta(\tau, z)$ is measured by using 20 equally spaced resistive wave gauges that are installed along the water tank at distances $z_j = 6j$ m, $j = 1, 2, \dots, 20$ from the wavemaker located at $z = 0$ m. This provides an effective measuring range of 120 m and a resolution of the k -spectrum of $2\pi/120$ rad m^{-1} (see “Methods”). The envelope $\psi(t, z = 0)$ of the

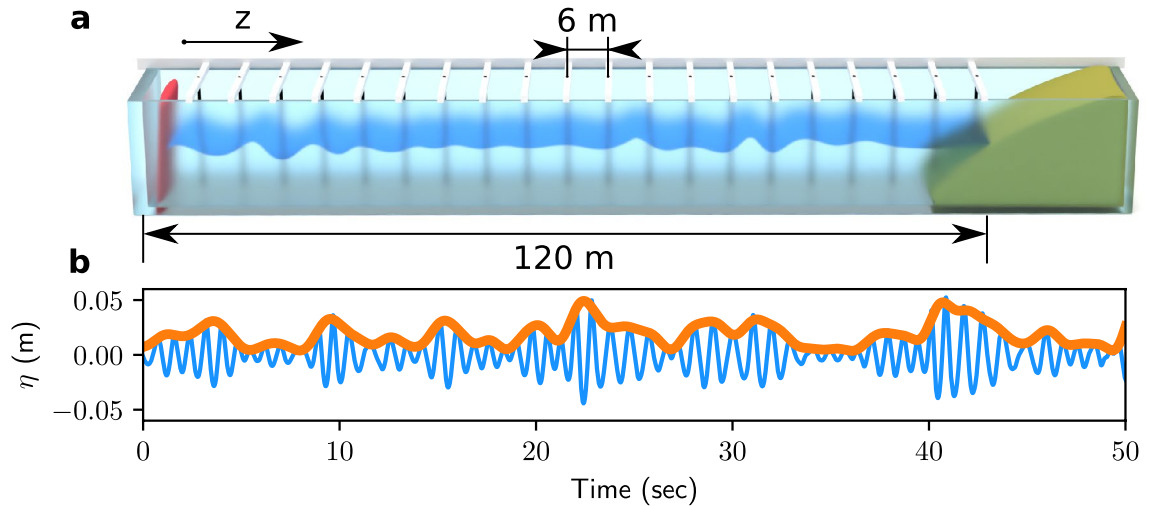


Figure 2. Experimental facility. **(a)** Schematic representation of the 120m-long water tank facility at École Centrale de Nantes. The surface elevation is recorded by a set of probes placed every 6 m of the water tank length. **(b)** Typical experimental wave train (surface elevation η , blue line) and its envelope (orange line) reconstructed by using the Hilbert transform.

surface elevation has a central frequency $f_0 = 1.15$ Hz and it is designed using the same procedure as the one used in our numerical simulations, i.e. by performing the linear superposition of a large number of independent random Fourier modes. The degree of nonlinearity is varied by changing either the averaged amplitudes or the initial spectral width Δf of the waves generated in the water tank.

A typical temporal evolution of the surface elevation experimentally recorded at the first gauge ($z = 6$ m) is plotted in the Fig. 2b. The slowly varying amplitude $\psi(z, t)$ is determined by using Hilbert Transform following techniques described, e.g., in Ref.²⁹. Typical spatio-temporal evolution of $|\psi|$ is plotted in Fig. 3a where we use the retarded time $t = \tau - z/c_g$. When Γ increases, we observe the emergence of pulses localized in space and time. The emerging pulses become narrower and most of them achieve a negative speed in the (t, z) diagram (see below).

As expected from our numerical simulations, the experimental PSD broadens and shifts toward the negative values of k (Fig. 3b). However, at high nonlinearity, the measured NDR deviates significantly from the numerical simulations and becomes asymmetric with ω . This phenomenon is the well-known “frequency downshift” of surface gravity waves induced by high order nonlinearities responsible for the negatives speeds observed in the (t, z) diagram shown in Fig. 3a³⁹. The numerical simulations of Dysthe equation (see below) and of the Euler equations (see Supplementary Material) confirm that this shape of the NDR is indeed induced by effects (not included in 1DNLSE) which break integrability of the wave equation.

Simulations of the Dysthe equation. The 1DNLSE (Eq. 2) is established under the assumptions of weak nonlinearity of the wave field as well as the narrowbandedness of its energy content. As it could be expected, at high values of the nonlinear parameter Γ , the measured NDR deviates from the one computed by performing numerical simulations of the 1DNLSE. The Dysthe equation (a higher-order nonlinear and not integrable generalized version of the 1DNLSE) provides a simple model that reproduces qualitatively the ω asymmetry of the NDR observed in experiments. Dysthe equation can be expressed as follows⁴⁰:

$$\frac{\partial \psi}{\partial z} + \frac{i}{g} \frac{\partial^2 \psi}{\partial t^2} + ik_0^3 |\psi|^2 \psi = \frac{k_0^3}{\omega_0} \left[\underbrace{6|\psi|^2 \frac{\partial \psi}{\partial t}}_a + \underbrace{2\psi \frac{\partial |\psi|^2}{\partial t}}_b - \underbrace{i\psi \mathcal{H} \left(\frac{\partial |\psi|^2}{\partial t} \right)}_c \right], \quad (6)$$

where \mathcal{H} stands for the Hilbert transform defined as follows: $\mathcal{F}(\mathcal{H}(f(t))) = -i \text{sign}(\omega) \mathcal{F}(f(t))$, where \mathcal{F} represents the Fourier transform and sign is the signum function. The extra terms labelled ‘a’, ‘b’ and ‘c’ in Eq. (6) represent higher order terms in a perturbative approach of Euler equation where the small parameter is the spectral width Δf . If $\Delta f \rightarrow 0$, the derivatives terms ‘a’, ‘b’ and ‘c’ vanish whereas the dominant cubic term $ik_0^3 |\psi|^2 \psi$ remains unchanged.

In order to investigate the influence of additional terms present in Dysthe equation, we have simulated the nonlinear propagation of identical initial conditions used in Fig. 1a, $\Gamma = 0.65$, including Dysthe terms labeled ‘a’, ‘b’, and ‘c’ separately as shown in Fig. 4. Parameters used in the numerical simulations are the same as those used for the numerical integration of the 1DNLE reported above.

As one can see in Fig. 4, the derivatives included in the terms ‘a’ and ‘b’ contribute to the nonlinear spectral shift, leading to the change of solitons’ group velocity (asymmetry in ω). The term ‘c’ reduces the shift of solitons

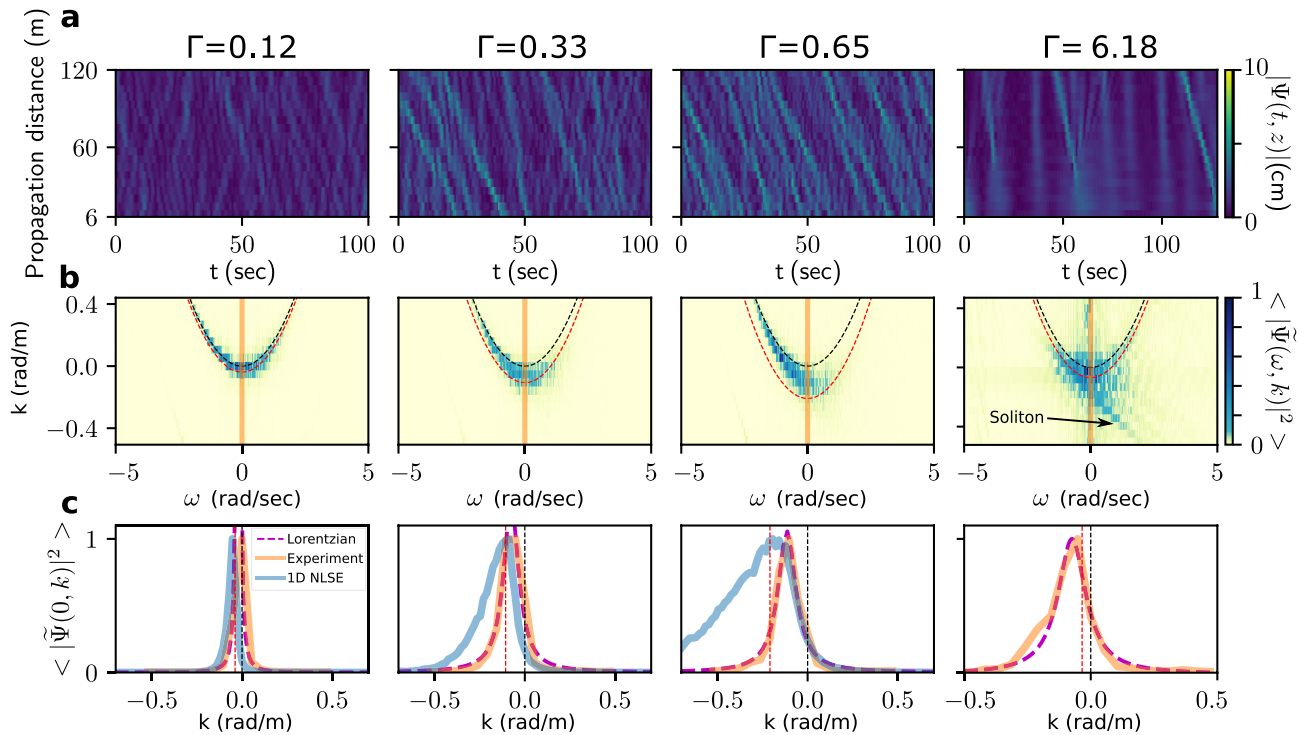


Figure 3. Experimental reconstruction of the nonlinear dispersion relation. Four columns correspond to four different values of Γ 0.12, 0.33, 0.65, and 6.18, respectively. **(a)** Spatiotemporal diagram of the wave envelope amplitude $|\Psi(t, z)|$. Data received from 20 probes have been post-processed and arranged in 20 vertical rows subtracting waves' group velocity ($t = \tau - z/c_g$). **(b)** Nonlinear dispersion relation reconstructed from the evolution of the complex wave envelope. $\Gamma = 0.12, 0.33, 0.65$ correspond to an initial spectral width $\Delta f = 0.2$ Hz and $|\tilde{\Psi}(\omega, k)|^2$ is averaged over several realizations (see "Methods"). In order to observe the signature of a single soliton, the NDR is not averaged for $\Gamma = 6.18$ (corresponding to $\Delta f = 0.037$ Hz). **(c)** Cross-section of the nonlinear dispersion relation at $\omega = 0$. Dashed purple line shows a Lorentzian fit, blue line shows corresponding results of NLS simulation.

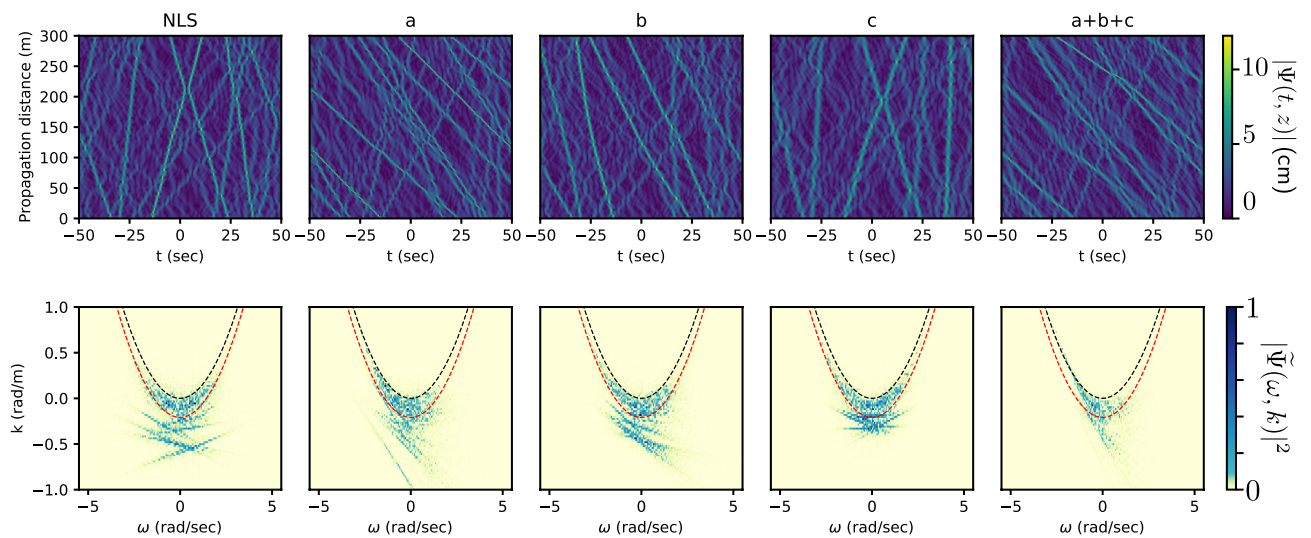


Figure 4. Numerical simulation of Dysthe model. Parameters correspond to Fig. 1a of the manuscript $\Gamma = 0.65$, $\varepsilon = 0.14$ (see "Methods"). Label 'NLS' corresponds to simulations of 1DNLS. Labels 'a', 'b', 'c', and 'a + b + c' indicate terms of Eq. (6) are added to the 1DNLS core.

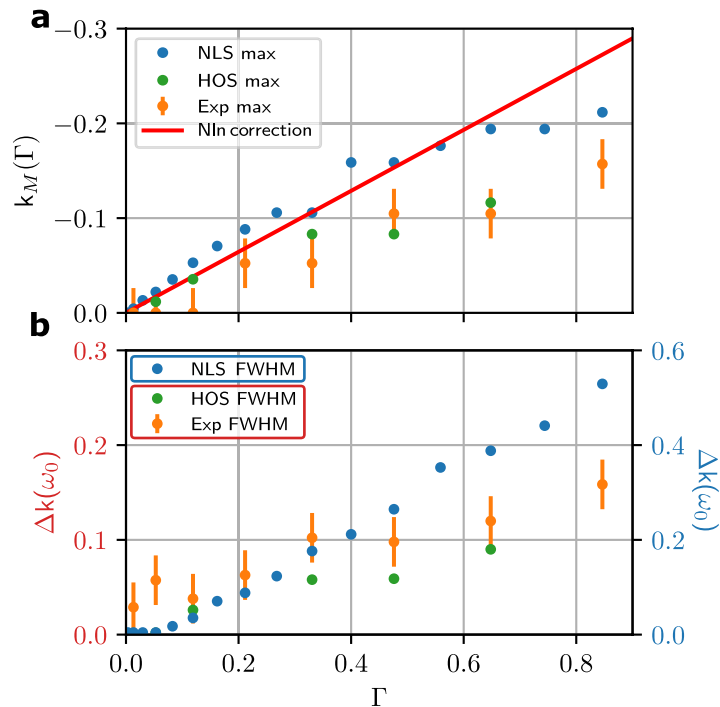


Figure 5. Quantitative comparison of the experimental results with different numerical models as a function of Γ . **(a)** Value of k at the NDR maximum for $\omega = 0$. Blue and green dots correspond to NLS and HOS simulations; orange dots show experimental data. Red line represents the theoretical curve (Eq. 5). **(b)** Full width at half maximum of the NDR for $\omega = 0$. Note that the vertical scale is different for experiments/HOS simulations (left scale) and 1DNLSE simulations (right scale). For all points in **(a,b)**, $f_0 = 1.15$ Hz, $\Delta f = 0.2$ Hz.

leading to a picture similar to 1DNLSE but with a smaller amplitudes of the localized structures which can be seen in the corresponding NDR plots.

Importantly, we have also run numerical simulations Euler equations by using high-order spectral (HOS) method (see Supplementary Material). The results of these simulations are close to those obtained with the Dysthe equation.

Nonlinear shift and broadening of the nonlinear dispersion relation. Our data analysis reveals that higher-order effects discussed above reduce the number of solitons embedded in random waves: indeed, we found that for $\Gamma \leq 1$, the straight lines in the (ω, k) space—signatures of solitons—appear much less frequently than in 1DNLSE simulations. Nevertheless, we have also observed these spectral signatures of solitons at extremely high nonlinearity (which is achieved with small values of the Δf , see the fourth column of Fig. 3).

The shapes of the PSD and of the NDR provide another signature of the deviation from IT: while the NDR predicted from the 1DNLSE becomes asymmetric at high nonlinearity, the experimental PSDs profiles $n_k = \langle |\tilde{\psi}(0, k)|^2 \rangle$ in Fig. 3c coincide with a Lorentzian fit for all values of Γ , a result also observed for HOS simulations.

The influence of the nonlinearity and of high order effects can be quantified with the help of the position $k = k_M(\Gamma)$ of the maximum and of the full width at half maximum $\Delta k(\Gamma)$ of n_k (see Fig. 5a,b respectively). Figure 5a shows that, both in experiments and simulations, $k_M(\Gamma)$ evolves more slowly than predicted by the weakly nonlinear theory—see Eq. (5). Moreover, because of the smaller number of solitons, the shift of the NDR toward negative values of k is weaker in experiments and HOS simulations than in IT (1DNLSE simulations).

Discussion

Our work provides new insight into the spectral properties of unidirectional nonlinear random waves. Our numerical simulations of the 1DNLSE show how the number of emerging solitons is directly related to the strength of nonlinearity in IT. Moreover, while a previous study has focused on the position of the maxima of the NDR²⁵, we also investigate the broadening of the NDR. Simulations reveal that the NDR provides a spectral signature of the solitons embedded in the random waves (asymmetric broadening in the k direction at high nonlinearity). Further investigations are needed to establish the theoretical link between the nonlinear spectra computed in the framework of IST and the broadening of the NDR (Fourier spectra).

From the experimental point of view, by focusing our analysis on the slowly-varying amplitude ψ , we were able to measure very accurately slight deviations from the predicted nonlinear dispersion relation. The results reported here provide new insights into an old fundamental problem of hydrodynamics: the measurement of the dispersion relation of random surface gravity waves (see for example⁵ and refs. therein). Various theoretical and

Ranges of ε	N	$L_{max} (m)$	N_{sample}
$\varepsilon \leq 0.05$	2048	500	10,000
$0.05 < \varepsilon \leq 0.09$	2048	500	500
$0.09 < \varepsilon \leq 0.19$	1024	2000	100

Table 1. Parameters of numerical simulations of 1DNLSE.

experimental works have been devoted to this question, see e.g.^{5,36,41–47}. For water tanks equipped with transparent side walls, cameras may be used to record the full spatio-temporal dynamics²³. Otherwise, a large number of gauges is needed⁵. The central point of our strategy is to remove the carrier wave frequency in order to retrieve the NDR of the slowly varying amplitude of waves having a narrow spectrum. Our simple experimental technique can be easily implemented in further investigations of the NDR of unidirectional water waves by using a very limited number of probes (20 probes here instead of 384 probes in⁵ for example, see “Methods”).

Our work contributes to the understanding of the NDR in nonlinear waves systems that involve solitons. Recently, a non trivial NDR has been established for finite gap solutions in the context of NLS soliton gases⁴⁸. The possible relationship between this NDR derived for soliton gases and the Fourier NDR studied here is an open fundamental question. On another side, the concept of NDR is receiving interest in the photonics community, where it has been for example recently used to explain the effect of dissipative soliton hopping in a photonic dimer⁴⁹ or to describe noise properties of a soliton frequency comb in a synchronously pumped cavity⁵⁰. In this article, we have demonstrated that the NDR measured in deep water waves experiments is close to the one predicted by using the 1DNLSE for low nonlinearity. For high nonlinearity, the measured NDR exhibits a signature of solitons but experiments deviates from IT because perturbative effects not taken into account in the 1DNLSE limit the emergence of solitons. It has been demonstrated that optical fiber experiments can be very close to integrability for high nonlinearity^{19,30}. The measurement of the NDR in optical fibers is extremely challenging but it has been recently demonstrated in a double loop fiber devices⁵¹. We hope that our work will also stimulate further investigation of the NDR of IT in photonics.

Methods

Nonlinear Schrödinger equation (1DNLSE). *Strength the nonlinearity: Benjamin-Feir index.* In order to compare nonlinearity and group velocity dispersion in the framework of the 1DNLSE (Eq. 2), it is useful to introduce a linear and a nonlinear propagation length as follows:

$$z_{lin} = \frac{g}{(2\pi \Delta f)^2} \quad \text{and} \quad z_{nlin} = \frac{1}{\gamma P_0}, \quad (7)$$

where Δf is a typical initial spectral bandwidth and $P_0 = \langle |\psi(t, z = 0)|^2 \rangle$ where $\langle \dots \rangle$ is the averaging over time and/or realizations. The degree of nonlinearity of the wave propagation is given by the parameter $\Gamma = z_{lin}/z_{nlin}$ (see Eq. 3).

Note that in the context of ocean waves, $\Gamma = \text{BFI}^2$ where BFI is the Benjamin-Feir Index^{31,32}. BFI index can also be expressed as follows:

$$\text{BFI} = \frac{\varepsilon}{(\Delta f/f_0)} = \sqrt{\Gamma}, \quad (8)$$

where $\varepsilon = k_0 \sqrt{2} \sigma$ is the wave steepness with $\sigma^2 = \langle \eta^2 \rangle = \langle |\psi|^2 \rangle / 2$ and Δf and f_0 are the average spectral width and the central frequency of the initial wave packets respectively.

Numerical simulations of 1DNLSE. In simulations and in experiments, the initial conditions are partially coherent waves made of the linear superposition of independent Fourier components at $z = 0$ and read:

$$\psi(t, z = 0) = \psi_0 \sum_{l=-N/2}^{+N/2} e^{-\frac{1}{2}(f_l/\Delta f)^2} e^{i2\pi f_l t} e^{i\phi_l} \quad (9)$$

where $f_l = l/T_{max}$, T_{max} is the temporal duration of the experiments and ϕ_l are independently and randomly distributed over $[0, 2\pi]$. Real part and imaginary part of such partially coherent waves exhibit Gaussian statistics at $z = 0$ (see²¹ for details).

Along the propagation in the focusing regime of 1DNLSE, the statistics deviates from Gaussianity and the probability density function of the wave amplitude becomes heavy-tailed. Note that the statistical characteristics of partially coherent waves are very different than plane waves initially perturbed by noise which is also investigated in²⁵. For a comparison between the two cases, refer e.g. to⁵².

Numerical simulations of Eq. (2) are realized using step-adaptive high order Runge-Kutta method. We construct different initial conditions using the random phase approach where a uniformly distributed phase is added to every Fourier component of a Gaussian spectrum with $\Delta f = 0.2$ Hz. Typical temporal windows used in the numerical simulations correspond to 100 seconds. Three parameters of simulations depend on the value of the steepness: the number of points N , the length of propagation L_{max} and the number of realizations N_{sample} . We separate the numerical studies into three ranges of steepness ε (see Table 1).

In order to reconstruct numerically NDR, we multiply the spatiotemporal diagram by a Super-Gaussian window with power 15 along z direction avoiding thereby undesirable effects related to the Fourier analysis of non-periodic signals.

Integrable turbulence: absence of non trivial resonances in the 1DNLSE. In general, WT is described by the resonant interactions among the Fourier components of the wave field^{53,54}. On the contrary, the non trivial resonances are forbidden in integrable turbulence^{20,55}. We consider the third order nonlinear interaction of four monochromatic waves $i = 1, 2, 3, 4$ of pulsation ω_i and wavenumber $k_i(\omega_i)$ in a unidirectional dispersive media. In this context, the resonances conditions of four wave mixing in the standard wave turbulence read $\omega_1 + \omega_2 = \omega_3 + \omega_4$ and $k_1 + k_2 = k_3 + k_4$ where $k_i = k(\omega_i)$ satisfies the *linear* dispersion relation $k(\omega)$. The linear dispersion relation of deep water waves is $k(\omega) = \omega^2/g$ and exact resonances thus lead to: $\omega_1^2 + \omega_2^2 = \omega_3^2 + (\omega_1 + \omega_2 - \omega_3)^2$ and then to: $\omega_1(\omega_3 - \omega_2) = \omega_3(\omega_3 - \omega_2)$. Finally, $\omega_1 = \omega_3$ and $\omega_2 = \omega_4$ or $\omega_2 = \omega_3$ and $\omega_1 = \omega_4$ *i.e.* exact resonances of non trivial interactions ($\omega_1 \neq \omega_3$ and $\omega_1 \neq \omega_4$) are forbidden.

Nonlinear dispersion of an isolated soliton. The fundamental soliton solution of the 1DNLSE (Eq. 2) reads⁵⁶:

$$\psi_S(t, z) = \psi_0 \operatorname{sech}[(t - c_s z)/\tau] \times \exp[i(k_s z - \omega_s t)] \exp[-iAz] \quad (10)$$

where the duration of the soliton is $\tau = \sqrt{2/(\gamma g |\psi_0|^2)}$. $k_s = k(\omega_s)$ obeys the linear dispersion relation, $c_s = c(\omega_s) = dk/d\omega = 2\omega_s/g$ is the group velocity of the soliton in the (z, t) plane and $A = \gamma |\psi_0|^2/2$. The double Fourier transform of $\psi_S(t, z)$ is given by:

$$\widetilde{\psi}_S(\omega, k) = 2\pi^2 \tau \psi_0 \operatorname{sech}[(\omega - \omega_s)\pi\tau/2] \times \delta\left[k - (k_s + (\omega - \omega_s)c_s - A)\right] \quad (11)$$

As a consequence, the NDR of a single soliton follows the straight line $k = c_s \omega + (k_s - c_s \omega_s - \frac{1}{2}\gamma |\psi_0|^2)^{25}$.

Measurement of the nonlinear dispersion relation

Resolution of the measurement of k . The key point in our approach is to remove the carrier wave before computing the NDR. This allows us to reveal the details of the NDR of the slowly varying envelop. In the water tank, the gauges are separated by 6 m and the maximum measurable wavevector is around 1.05 m^{-1} . As a consequence, contrary to Taklo et al. who use 384 probes, we do not resolve the wavevectors of the carrier wave $2\pi/\lambda_0 \simeq 5.3 \text{ m}^{-1}$ and of the harmonics. Our strategy enables the accurate measurement of the NLDR of the slow varying envelop of the wave by using only 20 probes. This provides an effective measuring range of 120 m with a resolution of the measurement of the k -spectrum of $\Delta k_{min} = 2\pi/120 \text{ rad m}^{-1}$. Note finally that, in⁵, the accuracy of the measurement of k given by the length of the water tank is $\Delta k_{min}/k_0 = 0.014$ while our setup enables an accuracy of $\Delta k_{min}/k_0 < 0.01$.

In order to measure the averaged spectra and NDR, we use 3, 6 and, 3 experimental runs with a duration of 512 s for $\Gamma = 0.12, 0.33, 0.65$, respectively. One run of 128 s have been used for $\Gamma = 6.18$.

Note that in NLS and HOS (high-order spectral, see Supplementary Material) simulations, the chosen lengths of propagation depend on the parameters and vary typically from 300 to 500 m. The uncertainty of measurement of k_M and Δk is therefore significantly lower in simulations than in experiments.

Evaluation of the full width at half maximum Δk of the position of the maximum k_M . In Fig. 4, we report the evaluation of the full width at half maximum Δk and of the position of the maximum k_M of the function $f(k) = |\widetilde{\psi}(k, \omega = 0)|^2$ in 1DNLSE, HOS simulations and in experiments. The accuracy of the measurement of Δk and k_M is limited both by the discretization of k (see above the uncertainty Δk_{min}) and by the random fluctuations of $f(k)$. In order to overcome these difficulties, when it is appropriate, we evaluate Δk and k_M by using best fitting procedure with Lorentzian function.

Data availability

The datasets generated and/or analysed during the current study are available in the *Figure data: Nonlinear dispersion relation in integrable turbulence* repository, <https://zenodo.org/record/6595429>.

Received: 19 April 2022; Accepted: 2 June 2022

Published online: 20 June 2022

References

1. Cobelli, P., Petitjeans, P., Maurel, A., Pagneux, V. & Mordant, N. Space-time resolved wave turbulence in a vibrating plate. *Phys. Rev. Lett.* **103**, 204301 (2009).
2. Herbert, E., Mordant, N. & Falcon, E. Observation of the nonlinear dispersion relation and spatial statistics of wave turbulence on the surface of a fluid. *Phys. Rev. Lett.* **105**, 144502. <https://doi.org/10.1103/PhysRevLett.105.144502> (2010).
3. Aubourg, Q. & Mordant, N. Investigation of resonances in gravity-capillary wave turbulence. *Phys. Rev. Fluids* **1**, 023701 (2016).
4. Hutchings, D. C., Sheik-Bahae, M., Hagan, D. J. & Van Stryland, E. W. Kramers-krönig relations in nonlinear optics. *Opt. Quantum Electron.* **24**, 1–30 (1992).
5. Taklo, T. M. A., Trulsen, K., Gramstad, O., Krogstad, H. E. & Jensen, A. Measurement of the dispersion relation for random surface gravity waves. *J. Fluid Mech.* (2015).

6. Deike, L., Bacri, J.-C. & Falcon, E. Nonlinear waves on the surface of a fluid covered by an elastic sheet. *J. Fluid Mech.* **733**, 394–413. <https://doi.org/10.1017/jfm.2013.379> (2013).
7. Carretero-González, R., Frantzeskakis, D. & Kevrekidis, P. Nonlinear waves in Bose–Einstein condensates: Physical relevance and mathematical techniques. *Nonlinearity* **21**, R139 (2008).
8. Benisti, D., Strozzi, D. J. & Gremillet, L. Breakdown of electrostatic predictions for the nonlinear dispersion relation of a stimulated Raman scattering driven plasma wave. *Phys. Plasmas* **15**, 030701 (2008).
9. Hager, R. & Hallatschek, K. The nonlinear dispersion relation of geodesic acoustic modes. *Phys. Plasmas* **19**, 082315 (2012).
10. Berhanu, M. & Falcon, E. Space-time-resolved capillary wave turbulence. *Phys. Rev. E* **87**, 033003. <https://doi.org/10.1103/PhysRevE.87.033003> (2013).
11. Hassaini, R. & Mordant, N. Transition from weak wave turbulence to soliton gas. *Phys. Rev. Fluids* **2**, 094803 (2017).
12. Ricard, G. & Falcon, E. Experimental quasi-1d capillary-wave turbulence. *EPL (Europhys. Lett.)*. <https://doi.org/10.1209/0295-5075/ac2751> (2021).
13. Novikov, S., Manakov, S. V., Pitaevskii, L. & Zakharov, V. E. *Theory of Solitons: The Inverse Scattering Method* (Springer, 1984).
14. Ablowitz, M. J., Kaup, D. J., Newell, A. C. & Segur, H. The inverse scattering transform-Fourier analysis for nonlinear problems. *Stud. Appl. Math.* **53**, 249–315 (1974).
15. Zakharov, V. E. Turbulence in integrable systems. *Stud. Appl. Math.* **122**, 219–234 (2009).
16. Walczak, P., Randoux, S. & Suret, P. Optical rogue waves in integrable turbulence. *Phys. Rev. Lett.* **114**, 143903 (2015).
17. Agafontsev, D. & Zakharov, V. E. Integrable turbulence and formation of rogue waves. *Nonlinearity* **28**, 2791 (2015).
18. Soto-Crespo, J. M., Devine, N. & Akhmediev, N. Integrable turbulence and rogue waves: Breathers or solitons?. *Phys. Rev. Lett.* **116**, 103901. <https://doi.org/10.1103/PhysRevLett.116.103901> (2016).
19. Tikan, A., Bielawski, S., Szwaj, C., Randoux, S. & Suret, P. Single-shot measurement of phase and amplitude by using a heterodyne time-lens system and ultrafast digital time-holography. *Nat. Photon.* **12**, 228 (2018).
20. Picozzi, A. *et al.* Optical wave turbulence: Towards a unified nonequilibrium thermodynamic formulation of statistical nonlinear optics. *Phys. Rep.* **542**, 1–132 (2014).
21. Randoux, S., Walczak, P., Onorato, M. & Suret, P. Nonlinear random optical waves: Integrable turbulence, rogue waves and intermittency. *Phys. D Nonlinear Phenomena*. <https://doi.org/10.1016/j.physd.2016.04.001> (2016).
22. El, G. & Kamchatnov, A. Kinetic equation for a dense soliton gas. *Phys. Rev. Lett.* **95**, 204101 (2005).
23. Redor, I., Barthélemy, E., Michallet, H., Onorato, M. & Mordant, N. Experimental evidence of a hydrodynamic soliton gas. *Phys. Rev. Lett.* **122**, 214502. <https://doi.org/10.1103/PhysRevLett.122.214502> (2019).
24. Suret, P. *et al.* Nonlinear spectral synthesis of soliton gas in deep-water surface gravity waves. *Phys. Rev. Lett.* **125**, 264101. <https://doi.org/10.1103/PhysRevLett.125.264101> (2020).
25. Leisman, K. P., Zhou, D., Banks, J., Kovačić, G. & Cai, D. Effective dispersion in the focusing nonlinear Schrödinger equation. *Phys. Rev. E* **100**, 022215 (2019).
26. Stokes, G. On the theory of oscillatory waves. *Trans. Camb. Philos. Soc.* **8**, 441–455 (1847).
27. Yuen, H. C. & Lake, B. M. Nonlinear dynamics of deep-water gravity waves. in *Advances in Applied Mechanics*. Vol. 22. 67–229. (Elsevier, 1982).
28. Bortolozzo, U., Laurie, J., Nazarenko, S. & Residori, S. Optical wave turbulence and the condensation of light. *J. Opt. Soc. Am. B* **26**, 2280–2284. <https://doi.org/10.1364/JOSAB.26.002280> (2009).
29. Osborne, A. *Nonlinear Ocean Waves* (Academic Press, 2010).
30. Suret, P. *et al.* Single-shot observation of optical rogue waves in integrable turbulence using time microscopy. *Nat. Commun.* **7** (2016).
31. Janssen, P. A. E. M. Nonlinear four-wave interactions and freak waves. *J. Phys. Oceanogr.* **33**, 863 (2003).
32. Onorato, M., Osborne, A. R., Serio, M. & Bertone, S. Freak waves in random oceanic sea states. *Phys. Rev. Lett.* **86**, 5831–5834 (2001).
33. Fedele, F., Cherneva, Z., Tayfun, M. & Guedes Soares, C. Nonlinear Schrödinger invariants and wave statistics. *Phys. Fluids* **22**, 036601 (2010).
34. El Koussaifi, R. *et al.* Spontaneous emergence of rogue waves in partially coherent waves: A quantitative experimental comparison between hydrodynamics and optics. *Phys. Rev. E* **97**, 012208 (2018).
35. Onorato, M., Proment, D., El, G., Randoux, S. & Suret, P. On the origin of heavy-tail statistics in equations of the nonlinear Schrödinger type. *Phys. Lett. A* **380**, 173–3177 (2016).
36. Longuet-Higgins, M. S. & Phillips, O. M. Phase velocity effects in tertiary wave interactions. *J. Fluid Mech.* **12**, 333–336 (1962).
37. Lvov, Y. V. & Onorato, M. Double scaling in the relaxation time in the β -Fermi-Pasta-Ulam-Tsingou model. *Phys. Rev. Lett.* **120**, 144301 (2018).
38. Bonnefoy, F. *et al.* From modulational instability to focusing dam breaks in water waves. *Phys. Rev. Fluids* **5**, 034802. <https://doi.org/10.1103/PhysRevFluids.5.034802> (2020).
39. Trulsen, K., Stansberg, C. T. & Velarde, M. G. Laboratory evidence of three-dimensional frequency downshift of waves in a long tank. *Phys. Fluids* **11**, 235–237 (1999).
40. Goullet, A. & Choi, W. A numerical and experimental study on the nonlinear evolution of long-crested irregular waves. *Phys. Fluids* **23**, 016601 (2011).
41. Whitham, G. Non-linear dispersion of water waves. *J. Fluid Mech.* **27**, 399–412 (1967).
42. Huang, N. E. & Tung, C.-C. The dispersion relation for a nonlinear random gravity wave field. *J. Fluid Mech.* **75**, 337–345 (1976).
43. Crawford, D. R., Lake, B. M. & Yuen, H. C. Effects of nonlinearity and spectral bandwidth on the dispersion relation and component phase speeds of surface gravity waves. *J. Fluid Mech.* **112**, 1–32 (1981).
44. Wang, D. W. & Hwang, P. A. The dispersion relation of short wind waves from space-time wave measurements. *J. Atmos. Ocean. Technol.* **21**, 1936–1945 (2004).
45. Gibson, R. & Swan, C. The evolution of large ocean waves: The role of local and rapid spectral changes. *Proc. R. Soc. A Math. Phys. Eng. Sci.* **463**, 21–48 (2007).
46. Leckler, F. *et al.* Analysis and interpretation of frequency-wavenumber spectra of young wind waves. *J. Phys. Oceanogr.* **45**, 2484–2496 (2015).
47. Taklo, T. M. A., Trulsen, K., Krogstad, H. E. & Borge, J. C. N. On dispersion of directional surface gravity waves. *J. Fluid Mech.* **812**, 681–697 (2017).
48. El, G. & Tovbis, A. Spectral theory of soliton and breather gases for the focusing nonlinear Schrödinger equation. *Phys. Rev. E* **101**, 052207 (2020).
49. Tikan, A. *et al.* Emergent nonlinear phenomena in a driven dissipative photonic dimer. *Nat. Phys.* **17**, 604–610. <https://doi.org/10.1038/s41567-020-01159-y>. arXiv:2005.06470. (2021).
50. Anderson, M. H. *et al.* Photonic chip-based resonant supercontinuum via pulse-driven Kerr microresonator solitons. *Optica* **8**, 771. <https://doi.org/10.1364/optica.403302> (2021).
51. Lechevalier, C. *et al.* Single-shot measurement of the photonic band structure in a fiber-based Floquet-Bloch lattice. *Commun. Phys.* **4**, 1–9 (2021).
52. Copie, F., Randoux, S. & Suret, P. The physics of the one-dimensional nonlinear Schrödinger equation in fiber optics: Rogue waves, modulation instability and self-focusing phenomena. *Rev. Phys.* **5**, 100037 (2020).

53. Zakharov, V. E., Lvov, V. S. & Falkovich, G. *Kolmogorov Spectra of Turbulence I: Wave Turbulence* (Springer, 2012).
54. Nazarenko, S. Wave turbulence. in *Lecture Notes in Physics*. <https://doi.org/10.1007/978-3-642-15942-8>. (Springer, 2011).
55. Suret, P., Picozzi, A. & Randoux, S. Wave turbulence in integrable systems: nonlinear propagation of incoherent optical waves in single-mode fibers. *Opt. Exp.* **19**, 17852–17863 (2011).
56. Yang, J. *Nonlinear Waves in Integrable and Nonintegrable Systems* Vol. 16 (SIAM, 2010).

Acknowledgements

This work has been partially supported by the Agence Nationale de la Recherche through the LABEX CEMPI project (ANR-11-LABX-0007), the ANR DYSTURB Project (ANR-17-CE30-0004), the ANR SOGOOD Project (ANR-21-CE30-0061-01) and the I-SITE ULNE (ANR-16-IDEX-0004), the Ministry of Higher Education and Research, Hauts de France council and European Regional Development Fund (ERDF) through the the Nord-Pas de Calais Regional Research Council and the European Regional Development Fund (ERDF) through the Contrat de Projets Etat-Région (CPER Photonics for Society P4S). E.F. is thankful for partial support from the Simons Foundation/MPS No. 651463.

Author contributions

All the authors contributed to the experiments and reviewed the manuscript. A.T., G.D. and F.B. performed numerical simulations.

Competing interests

The authors declare no competing interests.

Additional information

Supplementary Information The online version contains supplementary material available at <https://doi.org/10.1038/s41598-022-14209-7>.

Correspondence and requests for materials should be addressed to P.S.

Reprints and permissions information is available at www.nature.com/reprints.

Publisher's note Springer Nature remains neutral with regard to jurisdictional claims in published maps and institutional affiliations.



Open Access This article is licensed under a Creative Commons Attribution 4.0 International License, which permits use, sharing, adaptation, distribution and reproduction in any medium or format, as long as you give appropriate credit to the original author(s) and the source, provide a link to the Creative Commons licence, and indicate if changes were made. The images or other third party material in this article are included in the article's Creative Commons licence, unless indicated otherwise in a credit line to the material. If material is not included in the article's Creative Commons licence and your intended use is not permitted by statutory regulation or exceeds the permitted use, you will need to obtain permission directly from the copyright holder. To view a copy of this licence, visit <http://creativecommons.org/licenses/by/4.0/>.

© The Author(s) 2022